Enhanced oxygen evolution performance by partial phase transformation of cobalt/nickel carbonate hydroxide nanosheet arrays in Fe-containing alkaline electrolyte

Jinghua Liu[a], Hualan Li[b], Jiayang Cai[b], Jingyan Liu[c], Yansheng Liu[a], Zijun Sun[a], Xiong He[a,c], Dezhi Qu[b*], Xin Li[c*]*

[a] *Materials Science and Engineering Research Center, Guangxi University of Science and Technology, Liuzhou 545000, China*

[b] *Guangxi Key Laboratory of Green Processing of Sugar Resources, College of Biological and Chemical Engineering, Guangxi University of Science and Technology, Liuzhou 545006, China*

[c] *MIIT Key Laboratory of Critical Materials Technology for New Energy Conversion and Storage, School of Chemistry and Chemical Engineering, State Key Lab of Urban Water Resource and Environment, Harbin Institute of Technology, Harbin 150090, China.*

*Corresponding author: Tel.: +86-0451-86282153.

E-mail address: lixin@hit.edu.cn (X. Li), hexiong@gxust.edu.cn (X. He), qudezhi@gxust.edu.cn (D. Qu).

Table of content

Table S1 The chemical components for the synthesis of electrocatalysts 4

Fig. S1 XRD patterns of Co_1Ni_6CH before and after OER test. 4

Fig. S2 Elemental mapping images of Co_1Ni_6CH. 5

Fig. S3 (a) Low-resolution TEM image, insert high-resolution TEM image, and (b-g) elemental smart maps of Co1Ni6CH after OER test. 5

Table S2 The elemental composition of Co_1Ni_6CH before and after OER in KOH electrolyte from EDS spectra 5

Fig.S4 XPS spectra of NiCH and Co_1Ni_6CH. (a) XPS survey spectra, and (b) Ni 2p. 6

Table S3-1 The atomic composition of Co_xNi_yCH before OER derived from XPS. 6

Table S3-2 The atomic composition of Co_xNi_yCH after OER derived from XPS. 6

Table S3-3 The atomic composition of Co_1Ni_6CH in various electrolytes derived from XPS. 6

Fig.S5 Fe 2p XPS spectra of Co_1Ni_6CH after OER test. 7

Table S4 Comparison of OER activities for some cobalt-nickel based catalysts in alkaline solution 8

Fig.S6 Nyquist plots of these samples at the potential of 0.6 V vs. Hg/HgO. 9

Table S5 Related parameters for various electrodes before and after 1000 CV cycles 9

Fig.S7 CV curves of these samples in the potential range of 0.4-1.4 V vs. RHE. 9

Fig.S8 CV curves of these samples with various scan rates. 10

Fig. S9 (a) Mass activity curves, and (b) overpotential curves for various Co_xNi_yCH samples (solid lines represent samples before 1000 cycles, dash lines represent samples after 1000 cycles) 11

Fig. S10 (a)Polarization curves, and (b) Tafel curves for various Co_xNi_yCH samples (solid lines represent samples before 1000 CV cycles, dash lines represent samples after 1000 CV cycles) 11

Fig.S11 (a) Overpotential at 10 mA/cm2 in various electrolytes, and (b) plots showing the extraction of the Cdl for Co1Ni6CH in NaOH and Fe-free KOH electrolyte. 12

Fig. S12 (a)Polarization curves, and (b) Tafel curves for Co1Ni6CH samples in KOH, NaOH, and Fe-free KOH electrolytes (solid lines represent samples before 1000 CV cycles, dash lines represent samples after 1000 CV cycles) 12

Fig.S13 Nyquist plots of Co_1Ni_6CH in KOH, NaOH and Fe-free KOH electrolyte at the potential of

0.6 V vs. Hg/HgO. 13

Table S6 Related parameters for Co1Ni6CH in various electrolytes before and after 1000 cycles. 13

Fig. S14 Optimized structures of (a) NiOOH,(b) Co-NiOOH,(c) Fe-NiOOH, and(d) FeCo-NiOOH. 14

Fig. S15 Partial density of state of (a) NiOOH, (b) Co-NiOOH, (c) Fe-NiOOH, and (d) FeCo-NiOOH. 15

Table S1 The chemical components for the synthesis of electrocatalysts

Sample	$Ni(NO_3)_2$•$6H_2O$/g	$Co(NO_3)_2$•$6H_2O$/g	NH_4F/g	$CO(NH_2)_2$/g	H_2O/mL
NiCH	1.0905	----	0.2778	1.1261	100
Co_1Ni_9CH	0.9814	0.1092	0.2778	1.1261	100
Co_1Ni_6CH	0.9347	0.1559	0.2778	1.1261	100
Co_1Ni_1CH	0.5452	0.5458	0.2778	1.1261	100
CoCH	----	1.0915	0.2778	1.1261	100

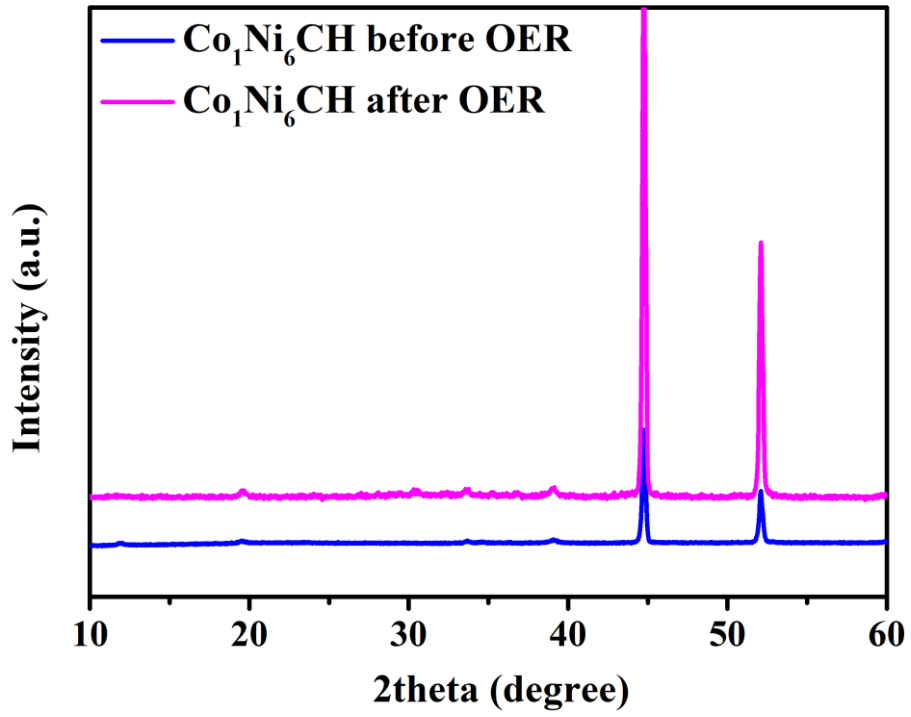

Fig. S1 XRD patterns of Co_1Ni_6CH before and after OER test.

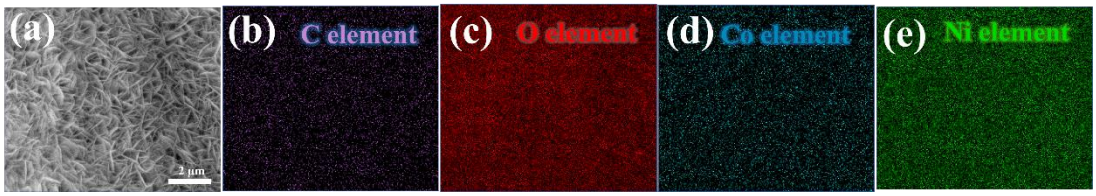

Fig. S2 Elemental mapping images of Co_1Ni_6CH.

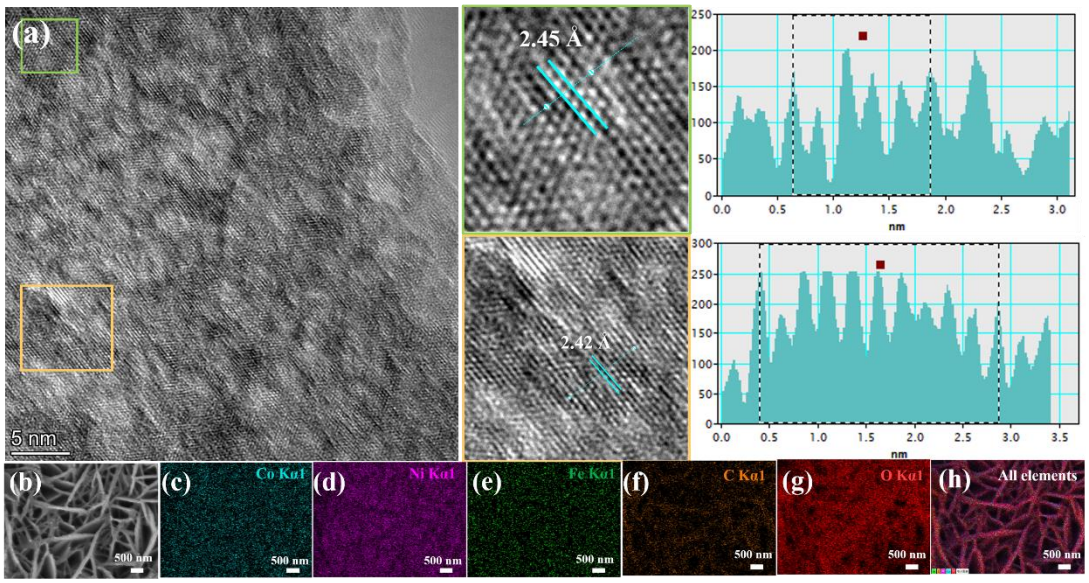

Fig. S3 (a) Low-resolution TEM image, (b) high-resolution TEM image, and (c-g) elemental smart maps of Co_1Ni_6CH after OER test.

Table S2 The elemental composition of Co_1Ni_6CH before and after OER in KOH electrolyte from EDS spectra

Sample	C (atom.%)	O (atomic %)	Co (atomic %)	Ni (atomic %)	Fe (atomic %)
Co1Ni6CH before OER	15.51	64.14	2.46	17.89	-----
Co1Ni6CH after OER	8.34	67.99	1.49	22.08	0.10

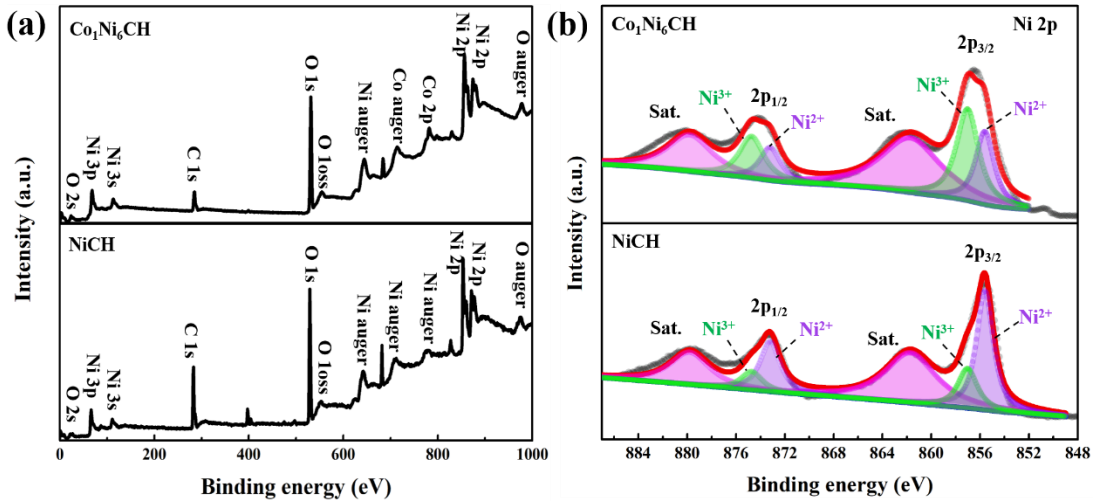

Fig.S4 XPS spectra of NiCH and Co_1Ni_6CH.
(a) XPS survey spectra, and (b) Ni 2p.

Table S3-1 The atomic composition of Co_xNi_yCH before OER derived from XPS.

	NiCH	Co_1Ni_1CH	Co_1Ni_6CH	Co_1Ni_9CH	CoCH
C (%)	20.75	16.45	17.51	19.69	24.87
O (%)	50.96	51.29	51.94	50.85	52.44
Ni (%)	28.29	24.28	26.72	25.92	---
Co (%)	---	7.98	3.83	3.54	22.69
Co/Ni	0/1	0.33/1	0.14/1	0.09/1	1/0

Table S3-2 The atomic composition of Co_xNi_yCH after OER derived from XPS.

	NiCH	Co_1Ni_1CH	Co_1Ni_6CH	Co_1Ni_9CH	CoCH
C (%)	27.81	22.97	26.05	21.61	19.57
O (%)	54.24	51.67	49.85	50.72	57.39
Ni (%)	16.63	18.44	19.84	23.9	---
Co (%)	---	5.72	2.5	1.83	21.17
Fe (%)	1.33	1.2	1.75	1.85	1.88
Co/Ni	0/1	0.31/1	0.13/1	0.08/1	1/0

Table S3-3 The atomic composition of Co_1Ni_6CH in various electrolytes derived from XPS.

	KOH	NaOH	Fe-free KOH
C (%)	26.05	32.37	26.48
O (%)	49.85	51.29	53.61
Ni (%)	19.84	14.06	17.52
Co (%)	2.5	1.44	1.64
Fe (%)	1.75	0.84	0.76
Co/Ni	0.13/1	0.10/1	0.09/1

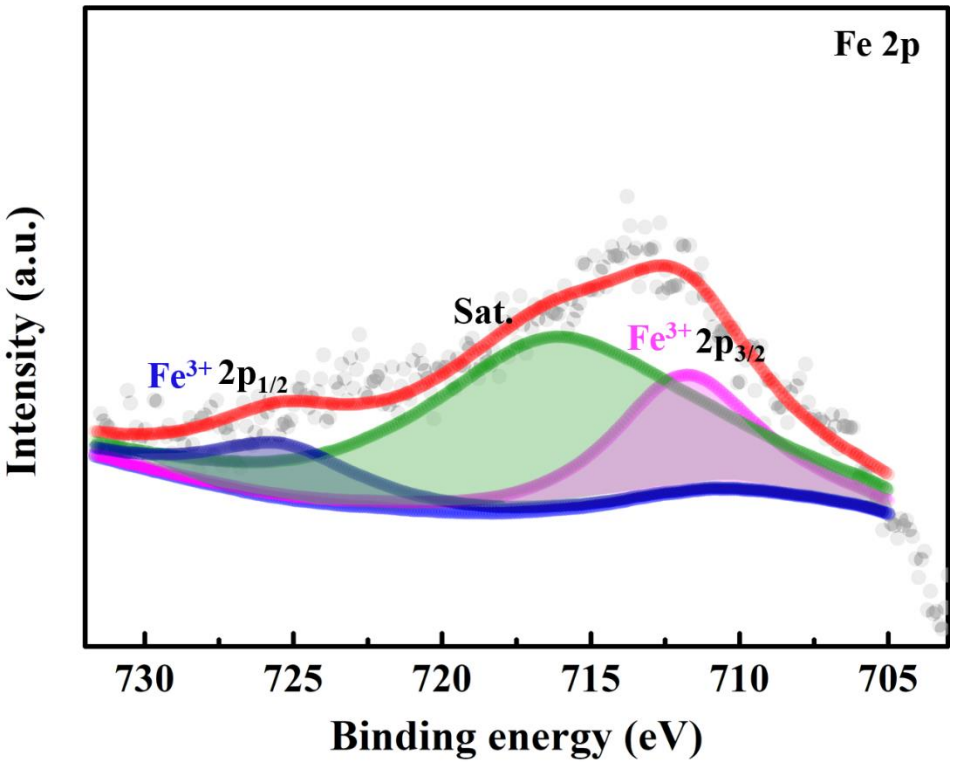

Fig.S5 Fe 2p XPS spectra of Co_1Ni_6CH after OER test.

Table S4 Comparison of OER activities for some cobalt-nickel based catalysts in alkaline solution

Catalyst	Electrolyte	Overpotential	Tafel slope	Ref.
Co_1Ni_6CH	**1 M KOH**	**256 mV (η50)**	**51**	**This Work**
$CoNi_{1.5}P$	1 M KOH	278 mV (η10)	67	[1]
$NiCo_2O$ HNS	0.1 M KOH	362 mV (η10)	64.4	[2]
Co_2Ni_1O	1 M KOH	310 mV (η10)	57	[3]
CoNiP-2	1 M KOH	277 mV (η10)	63.6	[4]
$CoNi_2S_4$	1 M KOH	260 mV (η10)	40.1	[5]
NiCoF-1,1	1 M KOH	~305 mV (η10)	77	[6]
NiCo-LDH	0.1 M KOH	~420 mV (η10)	113	[7]
CoNiSe	1 M KOH	380 mV (η100)	110	[8]
NiCoCH	1 M KOH	266 mV (η10)	44.8	[9]
NiCoCHH	1 M KOH	238 mV (η10)	190	[10]

Notice: HNS is hollow nanosponges, LDH is layered double hydroxide, CH is carbonate hydroxide, and CHH is Carbonate Hydroxide Hydrate.

Reference

[1] L.N. Zhou, L. Yu, C. Liu, Y.J. Li, Electrocatalytic activity sites for the oxygen evolution reaction on binary cobalt and nickel phosphides, RSC Adv., 10 (2020) 39909-39915.

[2] C.Z. Zhu, D. Wen, S. Leubner, M. Oschatz, W. Liu, M. Holzschuh, F. Simon, S. Kaskel, A. Eychmuller, Nickel cobalt oxide hollow nanosponges as advanced electrocatalysts for the oxygen evolution reaction, Chem. Commun., 51 (2015) 7851-7854.

[3] J. Zhao, X.R. Wang, X.J. Wang, Y.P. Li, X.D. Yang, G.D. Li, F.T. Li, Ultrathin porous nanosheet-assembled hollow cobalt nickel oxide microspheres with optimized compositions for efficient oxygen evolution reaction, Inorg. Chem. Front., 5 (2018) 1886-1893.

[4] L. Chai, S. Liu, S. Pei, C. Wang, Electrodeposited amorphous cobalt-nickel-phosphide-derived films as catalysts for electrochemical overall water splitting, Chem. Eng. J., 420 (2021) 129686.

[5] A. Sivanantham, P. Ganesan, S. Shanmugam, Hierarchical $NiCo_2S_4$ Nanowire Arrays Supported on Ni Foam: An Efficient and Durable Bifunctional Electrocatalyst for Oxygen and Hydrogen Evolution Reactions, Adv. Funct. Mater., 26 (2016) 4661-4672.

[6] Y. Xue, Y. Wang, H. Liu, X. Yu, H. Xue, L. Feng, Electrochemical oxygen evolution reaction catalyzed by a novel nickel–cobalt-fluoride catalyst, Chem. Commun., 54 (2018) 6204-6207.

[7] J. Jiang, A. Zhang, L. Li, L. Ai, Nickel–cobalt layered double hydroxide nanosheets as high-performance electrocatalyst for oxygen evolution reaction, J. Power Sour., 278 (2015) 445-451.

[8] D.X. Liang, J.X. Mao, P. Liu, J.W. Li, J.Y. Yan, W.B. Song, In-situ doping of Co in nickel selenide nanoflower for robust electrocatalysis towards oxygen evolution, Int. J. Hydrog. Energy, 45 (2020) 27047-27055.

[9] A. Karmakar, S.K. Srivastava, Transition-Metal-Substituted Cobalt Carbonate Hydroxide Nanostructures as Electrocatalysts in Alkaline Oxygen Evolution Reaction, ACS Appl. Energy Mater., 3 (2020) 7335-7344.

[10] K. Karthick, S. Subhashini, R. Kumar, S. Sethuram Markandaraj, M.M. Teepikha, S. Kundu, Cubic Nanostructures of Nickel–Cobalt Carbonate Hydroxide Hydrate as a High-Performance Oxygen Evolution Reaction Electrocatalyst in Alkaline and Near-Neutral Media, Inorg. Chem., 59 (2020) 16690-16702.

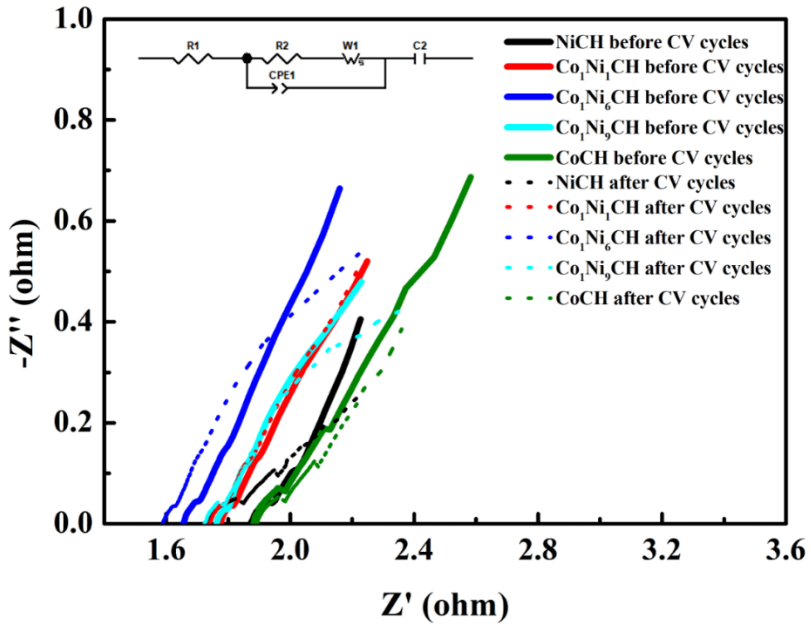

Fig.S6 Nyquist plots of these samples at the potential of 0.6 V vs. Hg/HgO.

Table S5 Related parameters for various electrodes before and after 1000 CV cycles

Samples before CV cycles	R1 (Ω)	R2 (Ω)	Samples after CV cycles	R1 (Ω)	R2 (Ω)
NiCH	1.863	0.580	NiCH	1.737	0.255
Co_1Ni_1CH	1.773	0.620	Co_1Ni_1CH	1.741	0.160
Co_1Ni_6CH	1.654	0.125	Co_1Ni_6CH	1.59	0.109
Co_1Ni_9CH	1.768	0.253	Co_1Ni_9CH	1.73	0.135
CoCH	2.00	0.685	CoCH	1.892	0.239

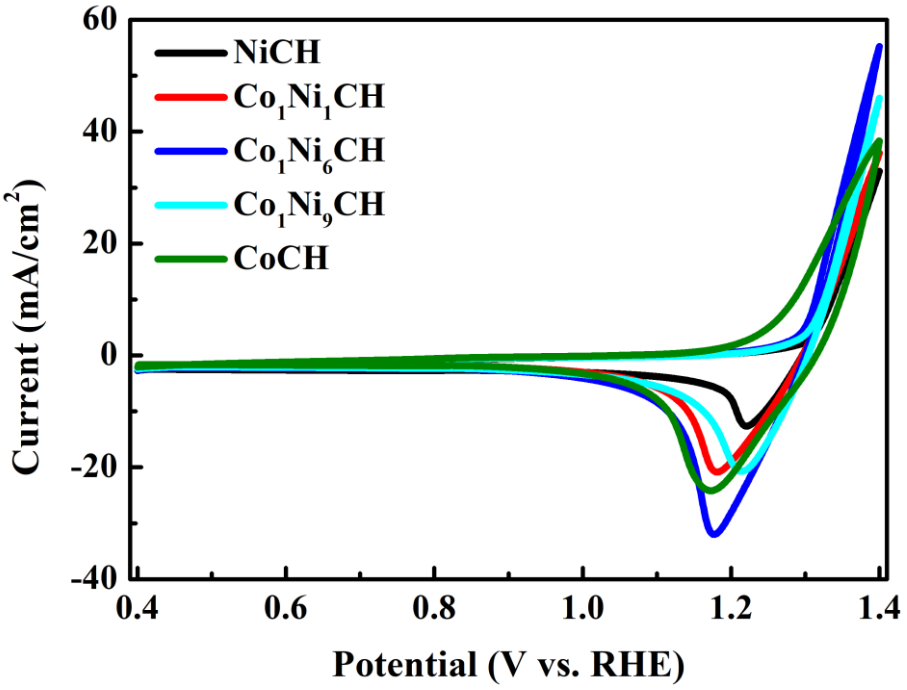

Fig.S7 CV curves of these samples in the potential range of 0.4-1.4 V vs. RHE.

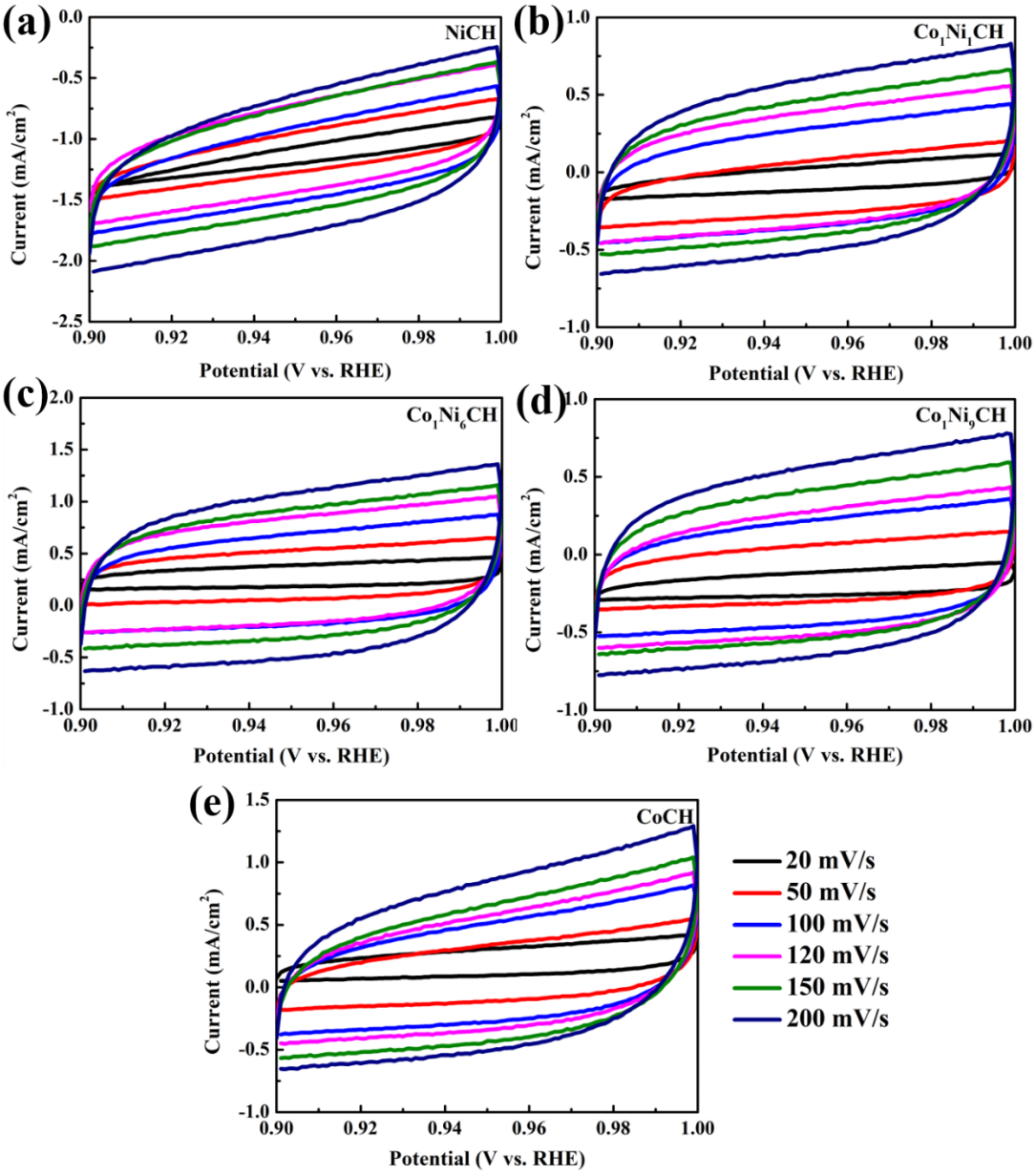

Fig.S8 CV curves of these samples with various scan rates.

Intrinsic activity calculation

1. The Turnover frequency (TOF) is defined as the number of O_2 molecules produced by each active site per second. It can be calculated as below:

$$TOF = \frac{Q}{4Fn}\ (s^{-1}) \qquad \text{Eq S1}$$

Where Q is the total charge that passes through the circuit in 1 s (Q = It, t = 1 s), F is the Faraday constant (F = 96485.3 C/mol), n is the number of moles of active sites. We assume that four electrons are required to give one O_2 molecule and 100% Faradaic efficiency were achieved. The mass loading of electrocatalysts in this work is about 1.4 mg. The electrocatalyst can be assumed as the formula of $M_2(OH)_2CO_3{\cdot}yH_2O$ (M is Ni,

Co, and Fe). Due to the partial phase transformation, $Ni_2(OH)_2CO_3 \cdot yH_2O$ is believed as the main existence. Thus, n can be obtained as below:

$$n = 2 \text{ x } \frac{1.4 \text{ x } 10^{-3}}{229.422} = 1.2 \text{ x } 10^{-5}\ mol \qquad \text{Eq S2}$$

In 1 M KOH, at overpotential = 250 mV, the OER currents are 5.6, 4.8, 32.4, 6.7, and 6.0 mA, respectively. The corresponding calculated TOF values are 0.0012, 0.0010, 0.0070, 0.0014, and 0.0013 s^{-1}.

2. Roughness factor (R_f) can be evaluated as below:

$$ECSA = \frac{C_{dl}}{C_s} \qquad \text{Eq S3}$$

$$Rf = \frac{ECSA}{A_g} \qquad \text{Eq S4}$$

Where C_{dl} is the double capacitance deduced from CV curves recorded in non-Faradic region, C_s exhibit the standard capacitance of atomically flat surface of the respective materials (C_s = 0.060 mF/cm^2). The active geometrical area of electrode is about 1 cm^2. The C_{dl} values from CV are 2.78, 2.68, 3.84, 3.00, and 3.19 mF/cm^2, respectively. Thus, the corresponding values of R_f are 46.33, 44.67, 64.00, 50.00, and 53.17.

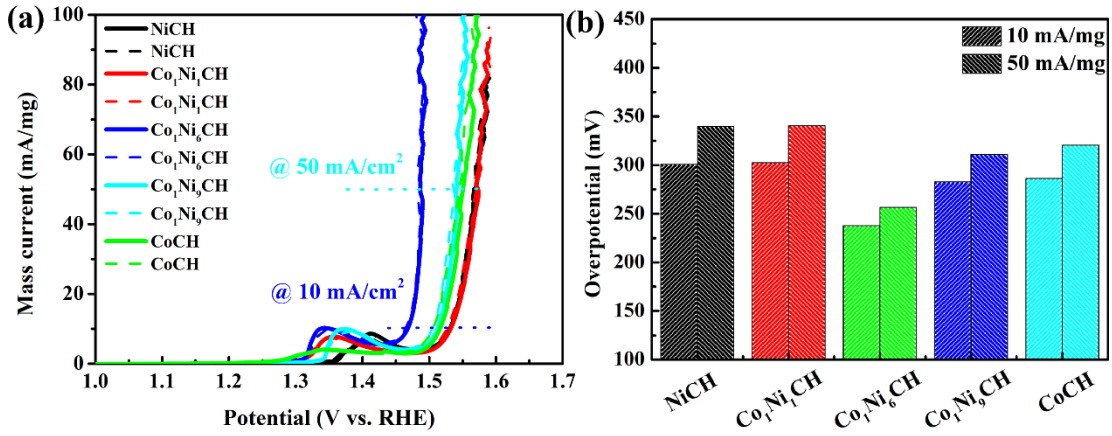

Fig. S9 (a) Mass activity curves, and (b) overpotential curves for various Co_xNi_yCH samples (solid lines represent samples before 1000 CV cycles, dash lines represent samples after 1000 CV cycles)

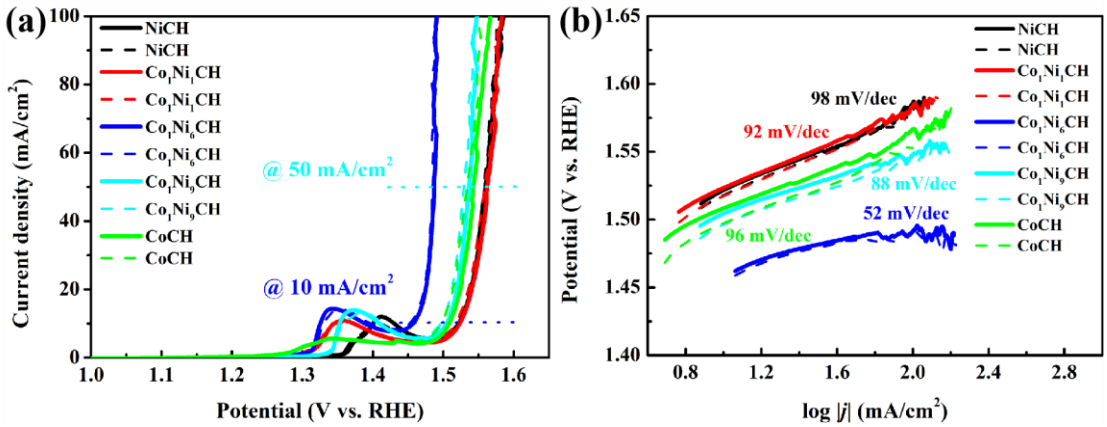

Fig. S10 (a)Polarization curves, and (b) Tafel curves for various Co_xNi_yCH samples (solid lines represent samples before 1000 CV cycles, dash lines represent samples after 1000 CV cycles)

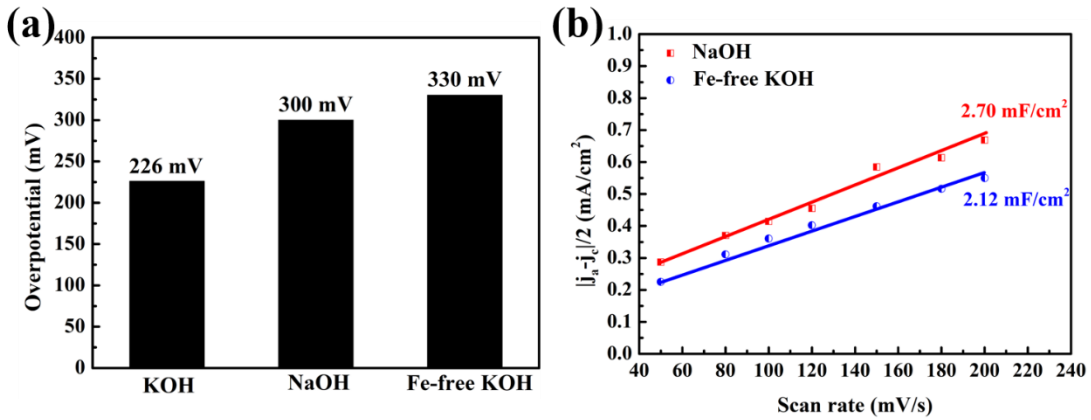

Fig.S11 (a) Overpotential at 10 mA/cm^2 in various electrolytes, and (b) plots showing the extraction of the C_{dl} for Co_1Ni_6CH in NaOH and Fe-free KOH electrolyte.

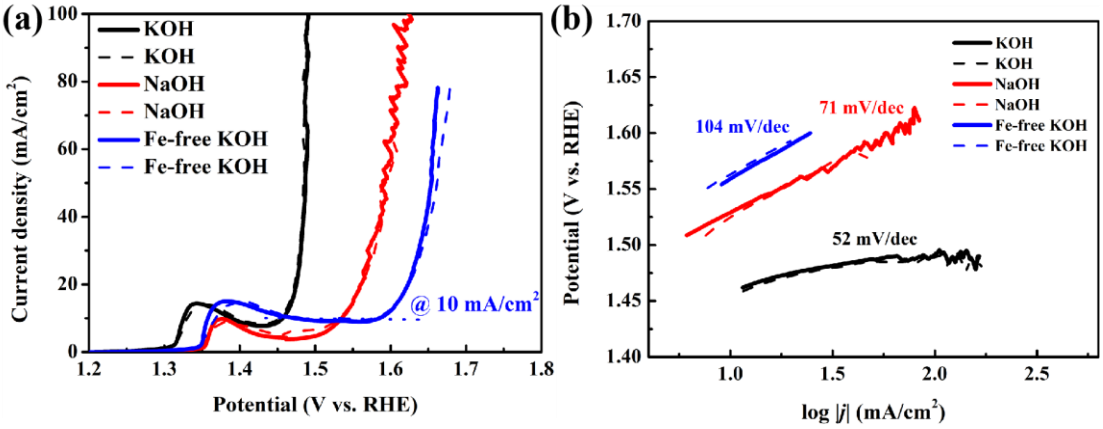

Fig. S12 (a)Polarization curves, and (b) Tafel curves for Co_1Ni_6CH samples in KOH, NaOH, and Fe-free KOH electrolytes (solid lines represent samples before 1000 CV cycles, dash lines represent samples after 1000 CV cycles)

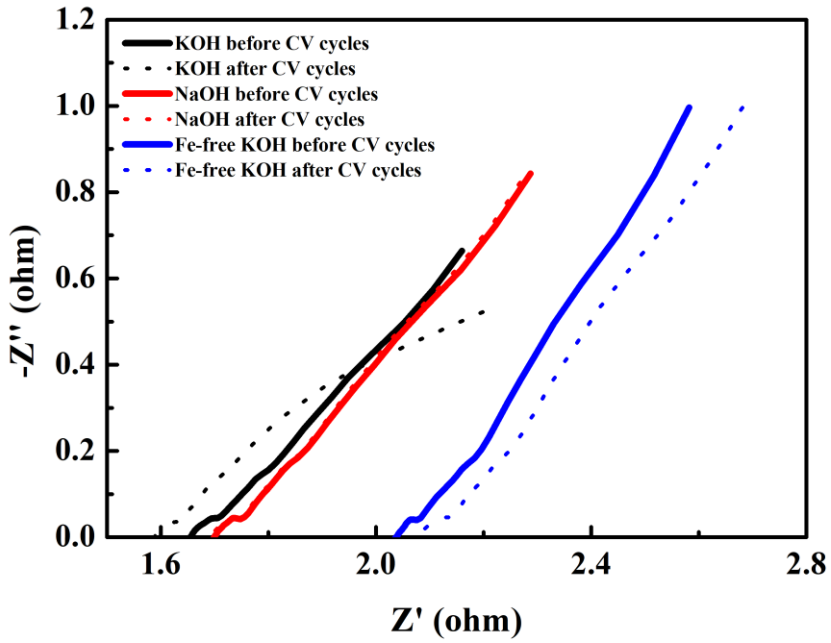

Fig.S13 Nyquist plots of Co1Ni6CH in KOH, NaOH and Fe-free KOH electrolyte at the potential of 0.6 V vs. Hg/HgO.

Table S6 Related parameters for Co1Ni6CH in various electrolytes before and after 1000 CV cycles

Samples before CV cycles	R1 (Ω)	R2 (Ω)	Samples after CV cycles	R1 (Ω)	R2 (Ω)
KOH	1.654	0.125	KOH	1.59	0.109
NaOH	1.70	0.197	NaOH	1.69	0.192
Fe-free KOH	2.038	0.143	Fe-free KOH	2.079	0.173

Calculation details

The Vienna Ab-initio Simulation Package (VASP) code using the projector augmented wave (PAW) method was used in the present density functional theory (DFT) calculations. The Generalized Gradient Approximation (GGA) of Perdew-Burke-Ernzerh (PBE) was used to describe the exchange and correlation energy density function. A slab model of the 4 × 4 unite cell is employed, and a 20 Å vacuum layer along the z direction are adopted to eliminate the interactions between the slabs. A 5 × 5 × 1 k-point mesh is used, and a cutoff energy of 520 eV is taken for expanding the wave functions into a plane-wave basis. The convergence for energy is chosen as 10-5eV between two steps and the maximum Hellmann-Feyman force acting on each atom is less than 0.01 eV/Å upon ionic relaxation.

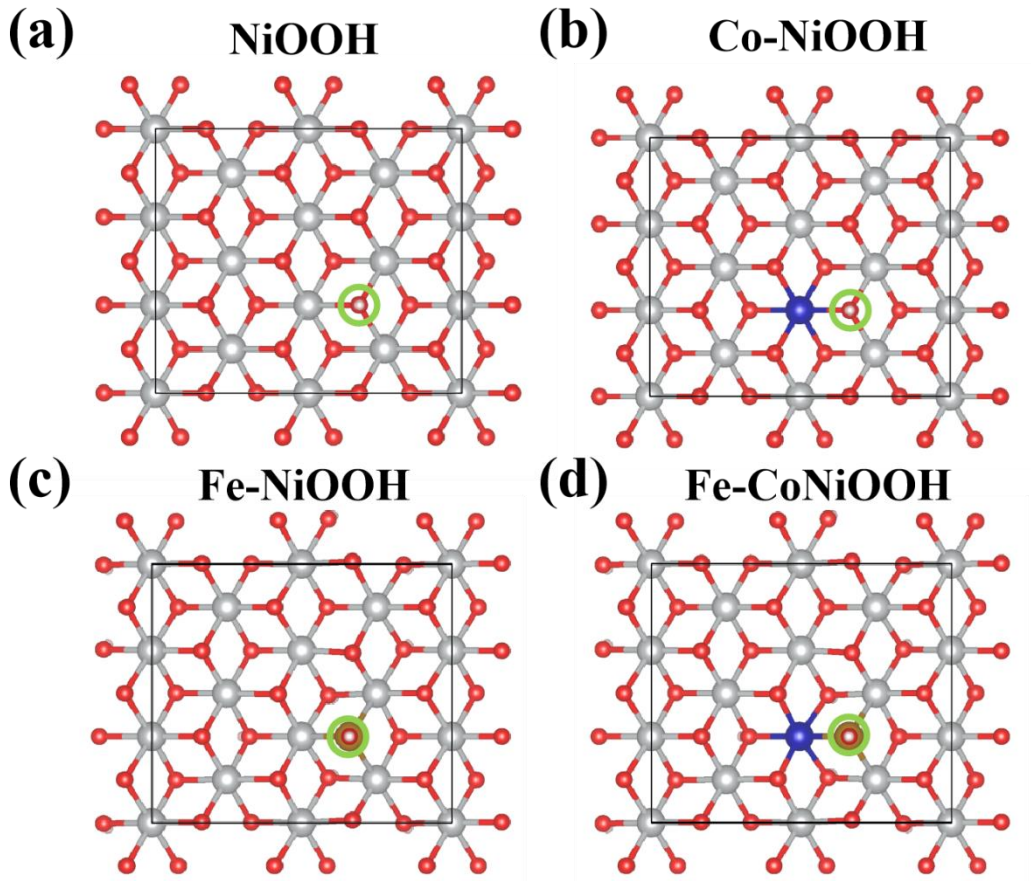

Fig. S14 Optimized structures of (a) NiOOH, (b) Co-NiOOH, (c) Fe-NiOOH, and (d) FeCo-NiOOH.

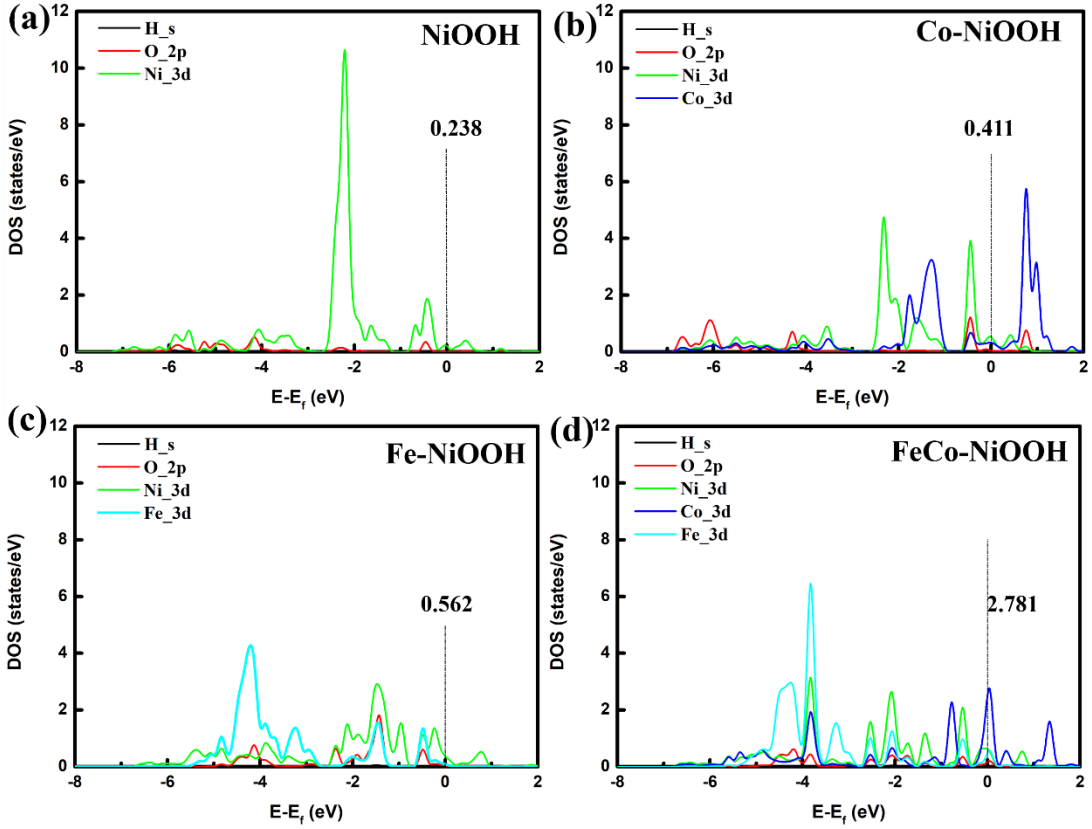

Fig. S15 Partial density of state of (a) NiOOH, (b) Co-NiOOH, (c) Fe-NiOOH, and (d) FeCo-NiOOH.